Nanoscale and Microscale Thermophysical Engineering, 18: 155–182, 2014

ISSN: 1556-7265 print / 1556-7273 online
DOI: 10.1080/15567265.2014.891680

TWO-DIMENSIONAL THERMAL TRANSPORT IN GRAPHENE: A REVIEW OF NUMERICAL MODELING STUDIES

Yan Wang, Ajit K. Vallabhaneni, Bo Qiu, and Xiulin Ruan
School of Mechanical Engineering and Birck Nanotechnology Center, Purdue University, West Lafayette, Indiana

This article reviews recent numerical studies of thermal transport in graphene, with a focus on molecular dynamics simulation, the atomistic Green's function method, and the phonon Boltzmann transport equation method. The mode-wise phonon contribution to the intrinsic thermal conductivity (κ) of graphene and the effects of extrinsic mechanisms—for example, substrate, isotope, impurities, and defects—on κ are discussed. We also highlight the insights from numerical studies aimed at bridging the gaps between 1D, 2D, and 3D thermal transport in carbon nanotubes/graphene nanoribbons, graphene, and graphite. Numerical studies on thermal transport across the interface between graphene and other materials and nonlinear thermal transport phenomena such as thermal rectification and negative differential thermal resistance are also reviewed.

KEY WORDS: graphene, two-dimensional, thermal transport, numerical modeling, phonon, molecular dynamics, Boltzmann transport equation, atomistic Green's function

INTRODUCTION

Low-dimensional carbon nanostructures, graphene and carbon nanotubes (CNTs) in particular, have attracted extensive scientific and engineering interest due to their special electronic [1–3], optical [4, 5], thermal [6, 7], and mechanical [8, 9] properties arising from the unique chemical and physical structure of these materials. Graphene, often referred to as a single layer of graphite, is an sp^2-bonded two-dimensional (2D) material of which the lattice structure is shown in Figure 1a. Graphene nanoribbon (GNR), a narrow strip of graphene possessing width and edge chirality–dependent band gap opening, has been suggested to have a versatile variety of applications [10, 11]. CNTs are another allotrope of carbon with a cylindrical nanostructure, of which the structure can be viewed as a GNR wrapped seamlessly into a cylinder. The chirality of GNRs and CNTs is determined by the shape of their edges, which can be zigzag, armchair, or chiral, as shown in Figure 1a.

Manuscript received December 20, 2013.

Address correspondence to Xiulin Ruan, School of Mechanical Engineering and Birck Nanotechnology Center, Purdue University, 585 Purdue Mall, West Lafayette, IN 47907. E-mail: ruan@purdue.edu

Current address for Bo Qiu: Department of Mechanical Engineering, Massachusetts Institute of Technology, Cambridge, Massachusetts

Color versions of one or more of the figures in the article can be found online at www.tandfonline.com/umte.

NOMENCLATURE

A	cross-sectional area
C_p	heat capacity
c	specific heat
d	diameter of carbon nanotube
G	thermal conductance
G_I	interfacial thermal conductance
$\hbar$	reduced Planck's constant
J	heat current
k	wave vector
k_B	Boltzmann constant
L	length
N	number of layers in multi-layer graphene
N_A	Avogadro's number
n	phonon occupation number
R_I	interfacial thermal resistance
Δ_r	root-mean-square height of edge variations in graphene nanoribbons
T	temperature
ΔT	temperature bias
∇T or $\vec{\nabla} T$	temperature gradient
t	time
V	volume
v_g	group velocity
w	width of graphene nanoribbons

Greek Symbols

α	exponent of the power law function for the length dependence of the thermal conductivity
δ	thickness of single-layer graphene or the wall of single-walled carbon nanotube, 0.335nm
η	thermal rectification ratio
Θ_D	Debye temperature
κ	thermal conductivity
λ	phonon mean free path
ν	index of phonon branches
Ξ	transmission function
ρ	mass density
τ	phonon relaxation time
ω	angular frequency

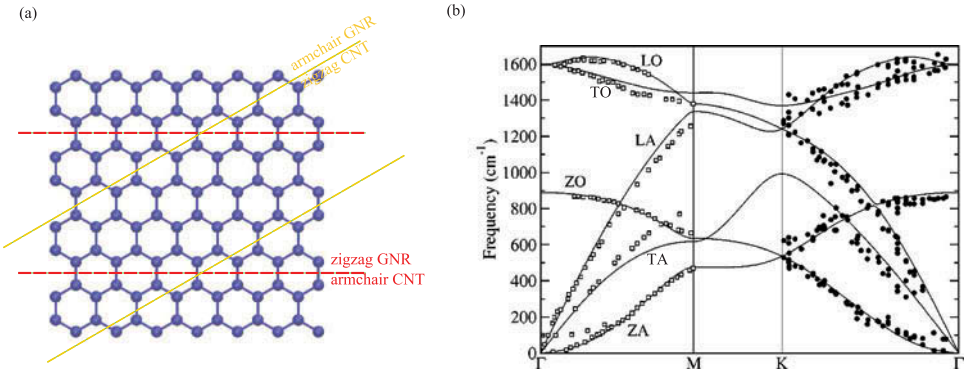

Figure 1 (a) Schematic of the lattice structure of graphene. Conceptually, GNRs can be cut from graphene into thin strips with zigzag (indicated by horizontal lines), armchair (indicated by inclined lines), or chiral (other directions) edges. CNTs can be viewed as rolling certain chiralities of GNRs into a seamless cylinder, with zigzag, armchair, or chiral edge chiralities. It is worth noting that a zigzag GNR is rolled into an armchair CNT and vice versa for armchair GNR and zigzag CNT. (b) The phonon dispersion relation of bulk graphene in the high symmetry directions. The solid lines are obtained using an *ab initio* force constant approach [12]. The open squares are data from an reflection electron energy loss spectroscopy experiment [13], and the solid circles denote results from a high-resolution electron energy loss spectroscopy measurement [14]. Panel (b) adapted from Dubay and Kresse [12], © American Physical Society. Reproduced by permission of American Physical Society. Permission to reuse must be obtained from the rightsholder.

Thermal transport in graphene and CNTs has been studied extensively since the last decade, due to their great value for fundamental science as well as practical issues such as increased power density in electronic components and self-heating in photonic devices. Compared to most three-dimensional (3D) materials, the low-dimensional structure and the strong C-C covalent bonds in graphene and CNTs give rise to distinctly different phonon dispersion and phonon–phonon scattering mechanisms in these materials, which altogether induces high thermal conductivity (κ) [15, 16]. The phonon dispersion relation of graphene consists of six branches: three polarizations, namely, flexural (Z), transverse (T), and longitudinal (L), for both acoustic (A) and optical (O) phonons, as shown in Figure 1b. The Brillouin zone (BZ) center phonon group velocities of TA and LA branches are four to six times higher than those in germanium or silicon. The out-of-plane atomic vibration in graphene—that is, the flexural mode—has a quadratic dispersion near the BZ center, which distinguishes them from most 3D materials that are characterized by a linear dispersion. The measured room temperature (RT) κ of single-layer graphene (SLG) is very high [7], indicating outstanding heat dissipation capability. However, the κs of suspended SLG measured by different groups span a wide range of 1,500-5,400 W/m-K [7, 17–20]. The κ of SLG supported by silica and copper substrates was found to be ~600 W/m-K [21] and 370^{+650}_{-320} W/m-K [22], respectively. Different defect concentrations, phonon–substrate scattering, as well as other factors were suggested to cause the large variations in the measured κ [23].

Numerical methods have been employed to explain many experimental observations. For instance, after the pioneering experimental observations [17, 21, 24], theoretical calculations have been used to reexamine the layer-number dependence of the κ of graphene [25], the thermal rectification in mass-graded carbon nanotubes [26], and the substrate effect on κ of graphene [27], which have provided rigorous analysis on thermal transport in these structures and provided mode-resolved phonon properties. Numerical studies have provided useful guidance for experimentalists as well; for example, a recent experiment [28] confirmed the width-dependent κ of GNRs predicted by numerical studies [29–32]. Chemically, GNRs and CNTs can be transformed into each other [33, 34]. Similarly, such links between graphene, GNRs, and CNTs in terms of thermal transport are also being built, particularly with computational efforts. The size dependence of κ in these low-dimensional materials is also of great interest to the scientific community, as an anomalously diverging κ in low-dimensional materials was predicted decades ago [35–37] though these theories have not been tested on realistic systems. In fact, there are still many valuable insights gained from numerical studies that have not been fully exploited or systematically combined to advance our understanding of thermal transport or aid the design of novel thermal materials, structures, or devices. This motivates us to summarize them in this review as a resource for both theorists and experimentalists. This review focuses on the 2D thermal transport in graphene, while CNTs and graphite are also briefly discussed for comparison purposes.

This article is organized as follows. The first section gives an overview on numerical methods for thermal modeling. The following sections are focused on graphene. First, we review numerical studies on the intrinsic κ, mode-wise decomposition of κ, and schemes for tuning the κ of graphene. The transition of phonon transport from 1D to 2D and from 2D to 3D are also discussed based on recent efforts in bridging the transport theory in CNT to that in graphene or that in SLG to graphite. Next we summarize recent progress on the research of thermal transport across solid–solid interfaces involving graphene. The following section

covers studies on the nonlinear transport phenomena in GNR based devices. Then we give an outlook toward the research in this field and conclude this review.

NUMERICAL METHODS FOR THERMAL TRANSPORT

In this section, we review a few numerical methods for modeling thermal transport in graphene, in particular, classical molecular dynamics (MD) simulations, the nonequilibrium Green's function (NEGF) method, and Boltzmann transport equation (BTE) methods in conjunction with phonon properties predicted via other tools; for example, density functional perturbation theory. These methods can either capture the thermal transport behavior from all phonon modes as a whole or track the contribution from a single phonon mode based on its relaxation time, mean free path (MFP), and velocity. They are appropriate for different phonon transport regimes or aspects because they deal with phonons in different manners, such as wave versus particle nature, time versus frequency domain, different thermodynamic conditions, and different boundary conditions (BCs).

Classical Molecular Dynamics Simulations

Classical MD simulations model the movements of atoms based on Newton's second law of motion and knowledge of the interatomic potentials. They can directly model phonon thermal transport and naturally account for atomic details of the structure such as defects, interface, strain, surface reconstruction, etc., which can provide atomic-level insights to thermal transport. Several MD schemes have been used for modeling heat transfer; for instance, nonequilibrium MD (NEMD) [38], reverse NEMD (RNEMD) [39], equilibrium MD (EMD) [38], thermal relaxation [40], the wave-packet (WP) method [41], and phonon normal mode analysis (NMA) [42, 43]. The accuracy of MD is limited by the quality of empirical interatomic potentials (EIP), and this has stimulated the invention of first-principles MD [44], which has also been applied to thermal modeling recently [45, 46]. The heat capacity in classical MD is the classical Dulong-Petit limit—that is, $C_p = 3N_A k_B$—which deviates from the quantum C_p at temperatures below the Debye temperature Θ_D. This is a drawback for high Θ_D materials like graphene [47].

Nonequilibrium and Reverse Nonequilibrium Molecular Dynamics NEMD and RNEMD methods [38, 39] are commonly used methods in computing the κ of materials. A constant temperature gradient ∇T is imposed across the simulation cell to generate a constant heat current J in the NEMD simulations and vice versa for RNEMD. Based on Fourier's law, κ can be computed as $\kappa = J/(\nabla T \cdot A)$, where A is the cross-sectional area of the simulated cell. In either NEMD or RNEMD, ∇T or J has to be maintained by two thermostats. The scattering of phonons by boundaries or thermostats should limit the phonon MFP λ as

$$\lambda^{-1} = \lambda_\infty^{-1} + L^{-1}, \tag{1}$$

where λ_∞ is the intrinsic phonon MFP in the bulk limit and L was taken as the distance between thermostats in Schelling et al. [38]. Such a size effect is significant for graphene, whose κ has a large contribution from phonons with long λ. An extrapolation method [38, 48] based on Eq. (1) has been recommended to compute the κ in the bulk limit; that is, extrapolating the κs of several simulation cells of different length to infinite length. These

methods are conceptually simple and easy to implement into MD simulations, and reasonable agreement with experiment can be achieved despite the unphysically large temperature gradient across the nanosized simulation domain [38]. A convergence study can be performed to ensure that the system is in the linear response regime where κ does not depend on ∇T. It should be noted that the use of Eq. (1) implicitly assumes that a finite bulk-limit λ and hence κ must exist, which may not be the case for certain low-dimensional systems of which the κ diverges with length [35–37]. Because NEMD and RNEMD are essentially the same despite the reversed cause-and-effect relation between J and ∇T, we will refer to both of them as NEMD in this review.

Green-Kubo Method The Green-Kubo method is commonly employed in EMD (we will refer to this method as GK-MD), which uses the heat current fluctuations to calculate κ based on the fluctuation-dissipation theorem [38, 49, 50]. Specifically, κ in the x direction can be computed as [49]

$$\kappa_x = \frac{1}{k_B V T^2} \int_0^\infty < J_x(t) J_x(0) > dt, \tag{2}$$

where k_B, V, t, and J_x denote the Boltzmann constant, volume of the simulation cell, time, and the heat current in the x direction. $< J_x(t)J_x(0) >$ is the heat current autocorrelation function (HCACF). We present the above formulation of the Green-Kubo method instead of the more frequently cited, isotropic one [38] because graphene, GNRs, and CNTs are anisotropic and hence Eq. (2) causes less confusion for the application to these materials. In addition to evaluating κ from the direct integral of the HCACF using Eq. (2), the HCACF can be fitted to an exponential decay curve first and then integrated [51]. So far, single [51], double [50], and triple [52] exponential fitting to the HCACF have been used to achieve acceptable fitting qualities. The finite size of the supercells used in EMD simulations can affect κ in GK-MD [53], and Wang et al. [30] also found that sufficiently long autocorrelation length is needed to accurately predict the κ of GNRs. Therefore, a convergence study on supercell size and autocorrelation length is needed.

Phonon Wave-Packet Method The phonon WP method is a straightforward way to capture the dynamic propagation and scattering of phonons by boundary, interface, defect, etc. At the beginning of the simulation, the atoms are displaced from their equilibrium positions accroding to a formular [41] that corresponds to a wave packet centered at a specific phonon mode (k, ω) of the material and standing at a specific position. Then the wave packet propagates toward the scatter at the group velocity of the corresponding phonon mode. By computing the total energy of the wave packet before and after its collision with the scattering center, the transmission coefficient can be evaluated. One limitation of the WP method is that it cannot capture anharmonic phonon scatterings due to the ~0 K simulation environment.

Normal Mode Analysis Similar to GK-MD, NMA is also used in EMD simulations. Based on the relaxation time approximation (RTA), NMA can be used to compute κ using the extracted phonon dispersion and spectral phonon relaxation time $\tau(k, \omega)$ [54]. The prediction of τ in NMA can be achieved in both the time domain [42, 55] by computing the decay rate of spectral energy and the frequency domain [56] by calculating the linewidth of spectral energy, of which the latter is the so-called spectral energy density (SED) analysis. Using the predicted mode-wise τ and v_g (from the phonon dispersion) for each phonon mode (k, ν), where ν denotes the index of phonon branches, κ can be evaluated under the RTA as

$$\kappa_x = \sum_k \sum_\nu c(k,\nu) v_{g,x}^2(k,\nu)\tau(k,\nu), \tag{3}$$

where the subscript x indicates the longitudinal direction. An advantage of this method over NEMD and GK-MD is that the the spectral v_g, τ, and λ can be computed, which gives more details of phonons.

Nonequilibrium Green's Function Method

Similar to the phonon WP method discussed above, the NEGF approach, sometimes referred to as the atomistic Green's function, also deals with the transmission of phonons. Unlike classical MD simulations, NEGF is valid at sub-Θ_D temperatures due to the quantum treatment of phonon distribution using the Bose-Einstein statistics. In NEGF, the transmission function $\Xi(\omega)$ across the system can be computed based on the Green's functions built from the interatomic force constants of the system. Details about the phonon NEGF approach can be found in Zhang et al. [57] and Wang et al. [58]. The heat flux and hence the thermal conductance can be computed using $\Xi(\omega)$ via the Landauer formula [57] as

$$J = \int \frac{\hbar\omega}{2\pi} \Xi(\omega) \left[n_1(\omega, T_1) - n_2(\omega, T_2)\right] d\omega \tag{4}$$

and

$$G = \left| \frac{1}{T_1 - T_2} \int \frac{\hbar\omega}{2\pi} \Xi(\omega) \left[n_1(\omega, T_1) - n_2(\omega, T_2)\right] d\omega \right|, \tag{5}$$

where n_1 and n_2 are the phonon occupation number of the two leads, which are at T_1 and T_2, respectively. This method can be referred to as "first-principles" if the force constants are extracted from density-functional theory (DFT) calculations. Force constants predicted from tight-binding calculations were also used in NEGF calculations [59]. For large systems containing hundreds of atoms or more, first-principles calculations of the force constant matrix are computationally forbidden, so the EIPs as those adopted by classical MD simulations have been used [60]. So far in most NEGF studies only the harmonic force constants have been used, limiting the credibility of such approaches to low temperatures at which the anharmonic phonon–phonon scattering is insignificant. Recently, anharmonic atomistic Green's function calculation has also been attempted [61].

Boltzmann Transport Equation

Based on the perturbation theory, the phonon BTE for a phonon mode i under a temperature gradient $\vec{\nabla}T$ is given as [49, 62]

$$-\vec{v}_{g,i} \cdot \vec{\nabla}T \frac{\partial n_i}{\partial T} + \left(\frac{\partial n_i}{\partial t}\right)_{collision} = 0, \tag{6}$$

which describes the balance of phonon population n (occupation number) between the diffusive drift (first term) and collision (second term, also refered to as scattering) of phonons. Several techniques for thermal transport modeling based on Eq. (6) has been developed [62, 63]. The most widely used are those based on the single-mode relaxation

time approximation (SMRTA), where every mode is assigned a relaxation time (τ_i) accounting for the net effect of different scattering mechanisms; that is, the collision term in Eq. (6) is approximated as

$$\left(\frac{\partial n_i}{\partial t}\right)_{collision} = \frac{n_{i,o} - n_i}{\tau_i}, \tag{7}$$

where $n_{i,o}$ is the occupation number of phonon mode i under thermal equilibrium; that is, the Bose-Einstein distribution. The relaxation time τ is the time constant for a phonon mode to return to its equilibrium occupation from a nonequilibrium one. SMRTA is only a first-order approximation to the phonon BTE, which neglects the deviation of τ from equilibrium values when the system is in nonequilibrium states. Beyond the SMRTA, Omini and Sparavigna [63] developed an iterative scheme that can solve the linearized Boltzmann equation accurately, which has been adopted by Broido and coworkers on phonon thermal transport in various solids, including graphene and CNTs, in the past few years [15, 16]. This method takes into account the modification to τ due to nonequilibrium population of all the phonons undergoing various scattering processes, so it does not suffer from the limitations of the SMRTA. For high-κ materials such as graphene and CNTs, the relaxation time of the Umklapp (U) process is strongly modified due to the shift of equilibrium phonon population by the strong normal (N) process. As a result, the iterative scheme is more accurate than SMRTA, especially for high-κ materials with strong N processes [64].

It is beneficial to make a comparison between this iterative BTE method with the NMA method discussed in the subsection on normal mode analysis because both methods deal with phonon scatterings spectrally. On one hand, the iterative BTE method is advantageous over the NMA method in that the former gives an accurate solution to the linearized phonon BTE, whereas the latter computes κ based on SMRTA. In addition, τ computed from NMA contains contributions from both N and U processes, so directly using the as-predicted τ tends to underestimate κ because only the U process directly contributes to thermal resistance. On the other hand, NMA has the advantage that it can capture the lattice anharmonicity to all orders, whereas the iterative BTE method is usually limited to first-order anharmonicity. Lindsay et al. have suggested that the neglect of higher-order anharmonicities could result in inaccurate prediction of the length-dependence of κ in SWCNTs [64].

THERMAL TRANSPORT IN GRAPHENE AND ITS DERIVATIVES

The measured high κ of graphene has sparked a lot of computational investigations aimed at gaining a deeper understanding of 2D thermal transport as well as exploring schemes for tuning it. In Table 1 we list the RT κ of graphene and graphite from numerical studies. As we can see, even the κ of the same structure can vary widely among studies. In particular, the κ values of SLG are in the range of 360–10,000 W/m-K, which encompass the experimental range mentioned in the Introduction.

Intrinsic κ of Graphene

In defect-free bulk materials, the phonon relaxation time τ and hence κ are solely determined by the anharmonic N and U processes, which are usually referred to as intrinsic scattering processes. For three-phonon scattering, the relations $\vec{k} + \vec{k}' + \vec{G} = \vec{k}''$ and

Table 1 Summary of computational results of κ of graphene and CNTs. The κs are adjusted according to the definition of the cross-sectional area as $A = \pi d\delta$, where $\delta = 0.335$ nm. Tersoff (TER) [65, 66], AIREBO (AIR) [67, 68], optimized Tersoff (OPT) [69] and Lennard-Jones (LJ) potential [70, 71] are EIPs for C-C interactions. Inter- and intralayer C-C interactions are denoted as Inter and Intra, respectively

Material	κ (W/m-K)	Method	Potential	Comments	Reference
SLG	~3,500	BTE	OPT	$L = 10$ μm	Lindsay al. [21, 25]
MLG, N = 2	~2,550	BTE	Intra:OPT Inter:LJ [70]	$L = 10$ μm	Lindsay al. [25]
Graphite	~2,350	BTE	Intra:OPT Inter:LJ [70]	$L = 10$ μm	Lindsay al. [25]
Graphite	480–850	GK-MD	Intra:OPT Inter:LJ [71]	κ depends on stacking order	Khadem and Wemhoff [72]
SLG	2,436	BTE	OPT	$L = 3$ μm	Lindsay et al. [16]
SLG	~1,950	NEMD	OPT	κ is from extrapolation	Qiu et al. [27]
SLG	~360	NEMD	AIR	κ is from extrapolation	Thomas et al. [73]
SLG	8,000–10,000	GK-MD	TER		Evans et al. [74]
SLG	1,626	SED	OPT		Qiu and Ruan [75]

$\omega(\vec{k}) + \omega(\vec{k}') = \omega(\vec{k}'')$ must be satisfied for momentum and energy conservation, where $\vec{G}$ is a translational vector of the reciprocal lattice with $\vec{G} = 0$ for an N process and $\vec{G} \neq 0$ for a U process. Other scattering processes such as boundary scattering and impurity scattering are refered to as extrinsic scattering processes.

In defect-free materials only the U process directly causes resistance to thermal transport; therefore, the N process was neglected in some BTE studies based on the SMRTA [76]. More recently, Lindsay et al. [15, 16] solved the linearized phonon BTE for graphene and CNTs including the N and U processes explicitly, and they observed that the N process can redistribute phonons to larger wave vectors for a U process, which is especially important for graphene and CNTs in which the U process is weak. Not all scattering processes satisfying the above conservation rules can happen in graphene and CNTs—selection rules enforce that acoustic modes can only participate in U processes involving optical modes in both graphene and CNTs, whereas for graphene, any scattering process involving an odd number of out-of-plane phonon modes is prohibited as the corresponding third-order derivatives of the interatomic potential are zero due to the reflection symmetry in graphene [15, 25]. Such selection rules strongly restrict the phase space for U scatterings and lead to the high κ of graphene and CNTs. Specifically, many U scattering processes involving the flexural phonons (ZA and ZO) in graphene are prohibited, which results in a high contribution of these phonon modes to κ in graphene [25, 77]. As shown in Figure 2a, the ZA contribution is ~74% at RT in Lindsay et al.'s work. It is even more important at low T due to its relatively lower energy than other modes, so that only ZA modes are excited.

Qiu and Ruan [75, 78] extracted τ and v_g of suspended and supported graphene (on amorphous silica) with SED analysis, and computed the mode-wise contribution to κ. In contrast to Lindsay et al. [15], Qiu and Ruan's calculation suggests roughly equal contribution from all acoustic branches in suspended graphene, as shown in Figures 2b and 2c. The discrepancy when comparing to the BTE results in Lindsay et al. [15] could arise from several factors, which have been discussed in the subsection on the Boltzmann transport equation.

Moderate ZA modes contribution to κ has also been reported in Chen and Kumar [79], where SED analysis shows that LA, TA, and ZA modes contribute 654, 330, and

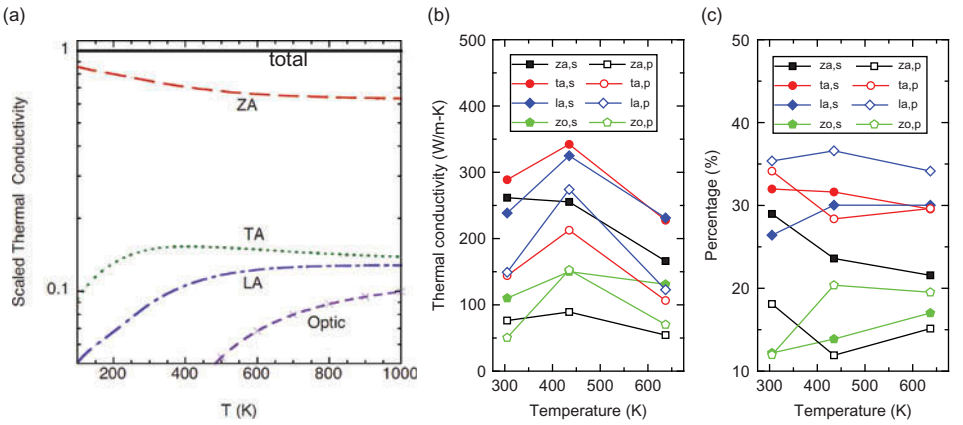

Figure 2 (a) Scaled thermal conductivity κ of different phonon branches normalized by the total κ as a function of temperature obtained from Lindsay et al.'s BTE calculation. (b) Contributions to κ from different phonon branches obtained from Qiu and Ruan's SED analysis [75], where the subscripts "s" and "p" stand for suspended and supported graphene, respectively. (c) Percentage contributions to κ from different phonon branches. (a) Panels reproduced from (a) Lindsay et al. [15], © American Physical Society. Reproduced by permission of American Physical Society. Permission to reuse must be obtained from the rightsholder.

361 W/m-K to κ, respectively. Similarly, Alofi and Srivastava studied mode-wise contribution to κ within the framework of Callaway's RTA model and the ZA contribution to RT κ was found to be ~50% [80].

All in all, despite the common belief that suspended graphene has high RT κ, the relative importance of different phonon branches to thermal transport is still under debate.

Length Dependence It was predicted that the intrinsic κ of 2D systems follows a logarithmic divergence with system size [37]. Though graphene possesses a 2D structure, the atoms can still vibrate in all three dimensions, which makes the size dependence of κ in such system mysterious. The length dependence of the RT κ of graphene and GNRs has been studied by both NEMD and BTE methods, though the conclusions differ among studies [15, 81–84].

Convergence of κ at a finite length was directly observed in Chen et al.'s NEMD simulations on supported graphene [82]. In Selezenev et al.'s NEMD simulation on suspended graphene [84], even though the κ was found to keep increasing with L, a linear relation between $1/\kappa$ and $1/L$ was obtained and the bulk limit value of κ was extracted based on the extrapolation scheme discussed in the subsection on NEMD and RNEMD, which indicates a converged κ with respect to length.

In constrast, in some studies [81, 83], κ of graphene and GNR was suggested to diverge with length in a power-law manner; that is, $\kappa \propto L^{\alpha}$, where α is between 0 and 1. Guo et al. [81] and Yu and Zhang [83] performed NEMD simulations and obtained power-law length-dependent κ for GNRs and, in particular, Guo et al. reported chirality dependence of α. Limited by the computational cost of MD simulations, fully diffusive thermal transport in graphene has not been directly modeled, so the size dependence remains an open question.

Lindsay et al. [15] observed that when the anharmonic phonon scatterings are only considered to the first order, κ diverges with length. They attributed the divergence to insufficient scattering to flexural modes due to the weak anharmonicity. Such divergence was

also reported in Lindsay et al. [64] for SWCNTs, while convergence was suggested if anharmonicity is considered to higher orders.

Substrate Effect: Perturbations from the Environment

Seol et al. [21] observed significantly reduced κ when graphene is supported on an SiO_2 substrate in their experiment. They also conducted BTE calculations with different TA-, LA-, or ZA-substrate interaction strengths to fit the κ-T curve. The best-fitting case, which has no TA- or LA-substrate interaction, reveals significant reduction of ZA contribution to κ and less but still considerable reduction of TA and LA contributions due to the leakage of ZA phonons that suppresses ZA+ZA $\rightarrow$ LA or TA conversions.

Ong and Pop [85] modeled supported graphene with MD simulations and reported a $>90\%$ reduction in κ. The SED analysis of suspended and supported graphene in their work shows significantly shortened τ of ZA in supported ones, whereas that of in-plane phonons is barely affected. Surprisingly, Ong and Pop found increasing κ with the graphene-substrate coupling strength, which was attributed to linearized phonon dispersion of the ZA branch due to substrate coupling. Such an effect cannot be captured by the BTE method used in Seol et al. [21] because it adopts a static dispersion.

Qiu and Ruan [75, 78] studied the graphene-on-silica problem with SED analysis, where they evaluated the substrate effect on the per mode τ, λ, and κ. Among all phonon branches, ZA modes see the greatest reduction in τ. Qiu and Ruan observed $\sim$67% reduction in RT κ for supported graphene. Specifically, they found considerable reduction of κ for all acoustic modes [78], whereas only a significant suppression of ZA was found in previous studies [15, 21, 85]. The discrepancies might be caused by the different EIPs used or methodological difference as discussed in the subsection on the Boltzmann transport equation.

It has been reported that the κ of supported graphene saturates at a moderate size, unlike suspended ones that show divergent κ even in micrometer scale due to the long λ of long wavelength phonons [75, 82]. This is reasonable since the phonon–substrate scattering is important and limits λ in the supported case. Qiu and Ruan [75] revealed a strong reduction of τ for long wavelength ZA phonons, which may explain the weakened size effect in supported graphene.

From Graphene to Graphite

Graphite is built with many graphene layers stacking together with vdW force either in a random stacking order (natural graphite) or in AB order (highly oriented pyrolytic graphite). The highest experimentally measured RT κ of suspended graphene has exceeded that of bulk graphite limit of $\kappa \approx 2,000$ W/m-K [87]. This raises the question of how the 2D thermal transport in SLG evolves to 3D in bulk graphite.

Ghosh et al. [17] measured the κ of graphene with layer numbers (N) ranging from 1 to 4 and a multilayer graphene (MLG) with approximately eight layers. They obtained monotonically decreasing κ with N and the κ of four-layer graphene already drops below the graphite limit. It is unknown whether the crossover is physical or due to uncertainties in the experiment. Ghosh et al. also performed theoretical calculations, which suggested that modified phonon dispersion and exponentially increasing number of U scattering should be the reason. Their model predicts monotonically decreasing κ from SLG to graphite, and κ eventually approaches the graphite limit in four-layer graphene.

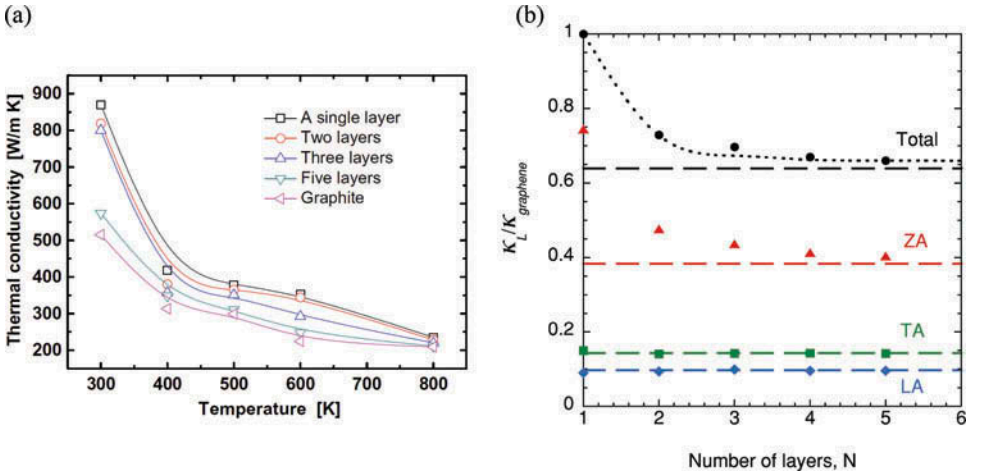

Figure 3 (a) κ of SLG, MLG, and graphite predicted from MD simulations. (b) Black circles denote the κ of MLG normalized by that of SLG for different number of layers (N). The per branch contributions by ZA (red triangles), TA (green squares), and LA (blue diamonds) branches are also shown. The corresponding graphite limit values are indicated by the horizontal dashed lines. Panels reproduced (a) Wei et al. [86], © Elsevier, Ltd. Reproduced by permission of Elsevier, Ltd, and (b) Lindsay et al. [25], © American Physical Society. Reproduced by permission of American Physical Society. Permission to reuse must be obtained from the rightsholder.

Classical MD simulations have been used to study thermal transport in multilayer graphene, graphite fiber, and multilayer GNRs, and κ decreasing and converging with increasing number of layer was obtained [84, 88, 89]. Wei et al. computed κ of SLG, MLG, and graphite using NEMD simulations [86]. As shown in Figure 3a, κ decreases monotonically with N.

Lindsay et al. [25] studied this problem considering the breaking of selection rules due to the interlayer coupling. They obtained monotonically decreasing κ with N, and κ saturates at the graphite limit when $N = 5$, as shown in Figure 3b. Specifically, they found that the thermal transport by TA and LA modes is barely affected, whereas that by ZA modes is suppressed by almost 50%, due to the same reason for supported graphene as discussed in the previous subsection, that is, breaking of selection rules for flexural modes. Similar conclusions were also made in Singh et al.'s work using a similar method [90].

It is interesting to make a comparison between the thickness dependence of the κ of thin films of conventional materials and that of MLGs. In thin films, phonon transport is limited by phonon–boundary scatterings in the thickness direction, resulting in an increasing κ with increasing film thickness. In contrast, phonon scattering by the rather specular surfaces of clean suspended MLG cannot induce enough boundary scattering, which is prevailed by other mechanisms, leading to decreasing κ with MLG thickness.

From Graphene to CNT: Effect of Curvature and Mode Quantization

Topologically, SWCNTs can be viewed as graphene strips rolled into a seamless cylinder. Thus, in principle, the properties of SWCNTs should approach those of a bulk graphene as its diameter d increases toward infinity.

Lindsay et al. [16] computed the κ of SWCNTs of various diameters extending to the graphene limit with the iterative phonon BTE method and found that, as d increases,

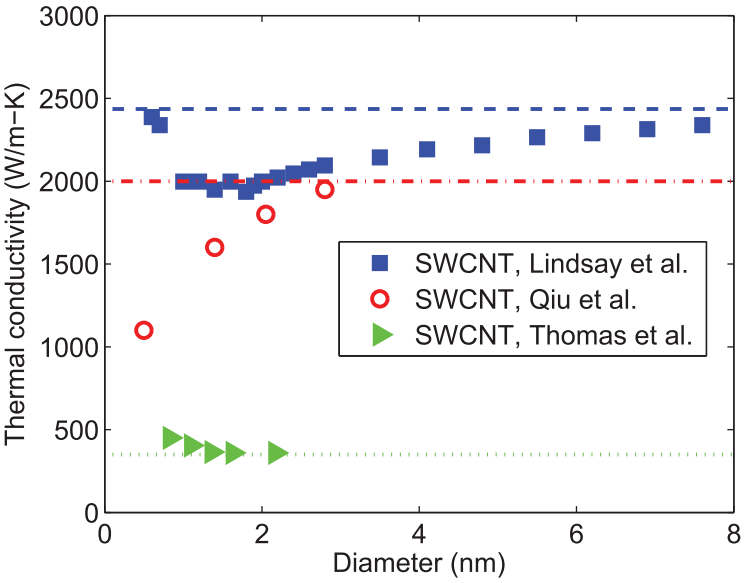

Figure 4 κ versus d for SWCNTs at RT. Blue squares are Lindsay et al.'s BTE results for zigzag SWCNTs [16]. Red circles are Qiu et al.'s NEMD results for zigzag SWCNTs [27]. Green triangles denote Thomas et al.'s NEMD results on armchair SWCNTs [73]. The horizontal lines denote the κ of bulk graphene computed in Lindsay et al. [16] (dashed), Qiu et al. [27] (dash-dot) and Thomas et al. [73], (dotted).

κ decreases with d for $d \lesssim 1.5$ nm and then increases with d until it saturates at the bulk graphene limit, as indicated by the solid blue squares and the dashed line in Figure 4. They attributed this trend to the competition between two mechanisms. First, as d increases, the number of optical phonon modes rises and their frequency moves toward the acoustic region, which causes more optical phonon scattering to acoustic phonons. This mechanism alone can reduce κ as d increases. Second, curvature breaks the reflection symmetry and correspondingly the selection rule; thus, more phonon scatterings can occur in thinner SWCNTs. This mechanism alone can induce an increasing κ as d rises.

Differently, Qiu et al. [27] obtained a monotonically increasing κ as d increases in their NEMD simulations, as shown in Figure 4. They attributed the inconsistency for thin SWCNTs between their work and Lindsay et al. [16] to the methodology difference discussed in the subsection on the Boltzmann transport equation. In some earlier MD simulations [73, 91, 92], however, κ of SWCNTs was found to decrease with increasing d, as shown in Figure 4 for Thomas et al.'s work [73]. Such disagreement was attributed by Qiu et al. [27] to the different EIPs used in previous studies.

Despite the difference in the trend of κ as d increases, the above studies agree with each other in that the κ of SWCNTs will finally converge to the bulk graphene limit, as we can see in Figure 4.

From Graphene to GNR: Edge Effect and Mode Quantization

The charality dependence of κ or G of GNRs has been studied with several methods [27, 29–32, 74, 93, 94] and most of them have predicted noticeable charality-dependent κ except Hu et al. [93] and Evans et al. [74]. Until now, the following observations are

mostly reported: (1) the κ of zigzag GNRs (zGNRs) is usually found to be higher than that of armchair GNRs (aGNRs); (2) the difference between κ_{zGNR} and κ_{aGNR} diminishes as the width of GNR increases; (3) κ increases toward the bulk graphene limit as the width increases.

Xu et al. [94] employed the NEGF method to compute the G of aGNRs and zGNRs with width up to 35 nm, where the difference between G_{zGNR} and G_{aGNR} decreases with width but it is still >10% for 35-nm-wide GNRs. They attributed the chirality dependence of G to the more localized lattice vibrations and less dispersive phonon bands in aGNRs. However, limited by the computational cost, no wider GNRs were studied and therefore no NEGF study has reported the width-converged G.

Aksamija and Knezevic [32] computed the κ of GNRs with width of 1 nm-10 μm using BTE considering U scattering and edge roughness scattering based on the SMRTA. The specularity of edges depends on the root mean square height of edge variations (Δ_r). The fact that $\Delta_{r,zGNR} < \Delta_{r,aGNR}$ leads to a higher roughness scattering rate at armchair edges, which results in lower κ of aGNRs than zGNRs. Aksamija and Knezevic [32] demonstrated diminishing chirality dependence of κ when the ribbon width increases from ~1 nm to 10 μm, and the κ of both aGNR and zGNR converges to the bulk graphene limit.

Wang et al. [30] studied the edge effect in GNRs using GK-MD simulations. With phonon spectra analysis, they found more significant localization of flexural phonons at the edges of aGNRs than those of zGNRs, as indicated by Figures 5a–5c, and the thermal transport near edges is seriously suppressed.

Wei et al. [95] investigated phonon scattering at GNR edges with the WP method. They found almost specular phonon reflection at zigzag edges while considerable diffuse reflection at armchair ones, as shown in Figures 5d and 5e, and the diffuse reflection at armchair edges is stronger for ZA modes than TA and LA modes. It should be noted that various factors can induce such differences in phonon scattering at armchair and zigzag edges; for example, mode quantization [94], roughness scattering [31] and phonon localization [30].

It is worth mentioning that Bae et al. [28] recently measured the κ of supported GNRs of various width, and they found that κ keeps increasing even in 130-nm-wide ones. The authors' BTE simulations suggests the existence of edge-scattering mechanisms other than roughness scattering, such as the edge-roughness correlation used in Aksamija and Knezevic [32] or the edge phonon localization mechanism proposed in Wang et al. [30]. It is possible that the edge effect in GNRs could be due to a combination of the mechanisms mentioned above. For very narrow GNRs (<10 nm), width and chirality have a great influence on phonon spectra due to phonon mode quantization, whereas for wide GNRs (>100 nm), the dispersion relation can be considered to recover that of bulk graphene's, so edges manifest themselves as perturbation, and hence the mechanisms affecting phonon-edge scattering would be more important.

Isotope and Defect: Lattice Disorders

There are two stable isotopes of carbon in nature—^{12}C and ^{13}C, comprising ~99% and ~1% of naturally occurring carbon materials, respectively. Unless deliberately engineered, ^{12}C and ^{13}C atoms are randomly arranged in graphene and CNTs. Isotopic manipulation of graphene has been investigated and significant modification of its thermal properties has been reported [96, 97]. On the other hand, there are many forms of defects in graphene; for instance, single vacancy, di-vacancy, Stone-Wales, and substitutional defects like donor and acceptor elements, etc. Unlike isotopes, which only introduce

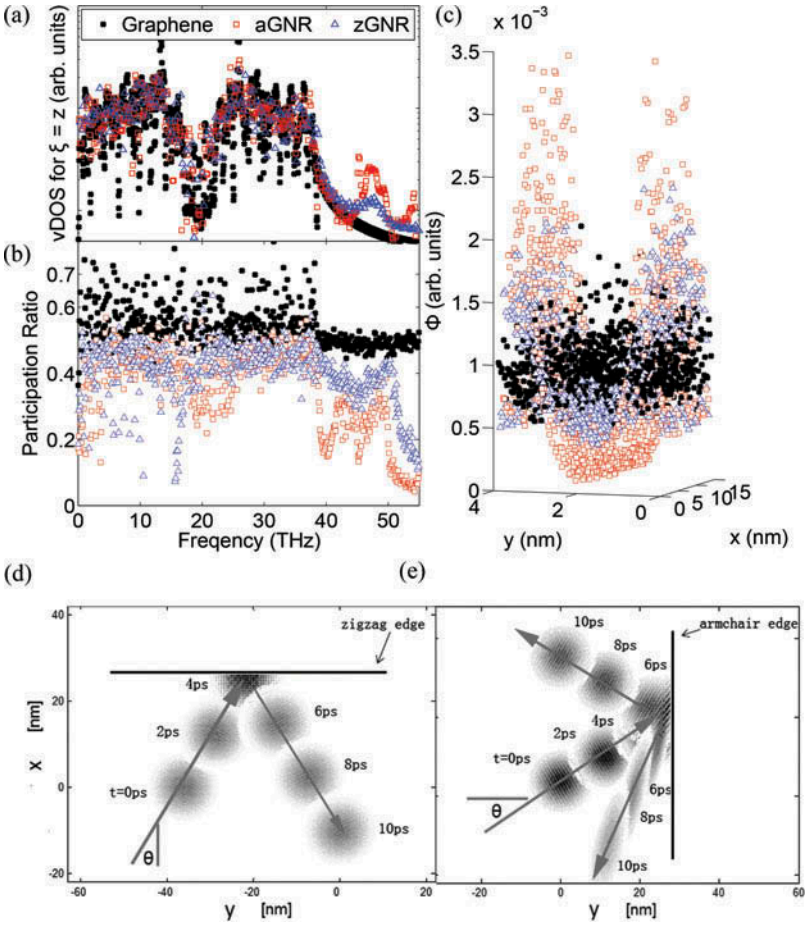

Figure 5 (a), (b), and (c) are phonon spectra analysis results on graphene, zGNR, and aGNR. (a) The vibrational density of states. (b) The phonon participation ratio. (c) The spatial distribution of localized modes. More localized phonons can be found at armchair edges than zigzag ones. (d) and (e) show the propagation history of a phonon wave-packet (ZA branch) incident at the zigzag (d) and armchair (e) edges of a GNR. Considerable phonon backscattering can be seen in (e). The x and y axes in panels (c), (d), and (e) denote the coordinates. Panels reproduced (a), (b), and (c), Wang et al. [30]; (d) and (e) Wei et al. [95]. © AIP Publishing, LLC. Reproduced by permission of AIP Publishing, LLC. Permission to reuse must be obtained from the rightsholder.

a mass difference to the mother structure, defects can distort the lattice in a stronger way so as to induce stronger modification to phonon transport than isotopes [31, 98]. The practical importance of the research on how isotopes and defects influence thermal transport in graphene and CNTs can be manifested in several aspects. First, isotopic engineering offers a way that allows tailoring thermal properties without disturbing electron transport. Such decoupled engineering of thermal and electrical properties is especially useful in nanoelectronics. Second, the intentional or unintentional introduction of defects such as donors, acceptors, and vacancies into graphene and CNTs is common in many applications, and its effect on thermal transport needs to be understood for thermal management of the devices. Third, there have been consistent efforts in exploiting the unique thermoelectric and electrical properties of graphene and CNTs to develop high-performance thermoelectric materials

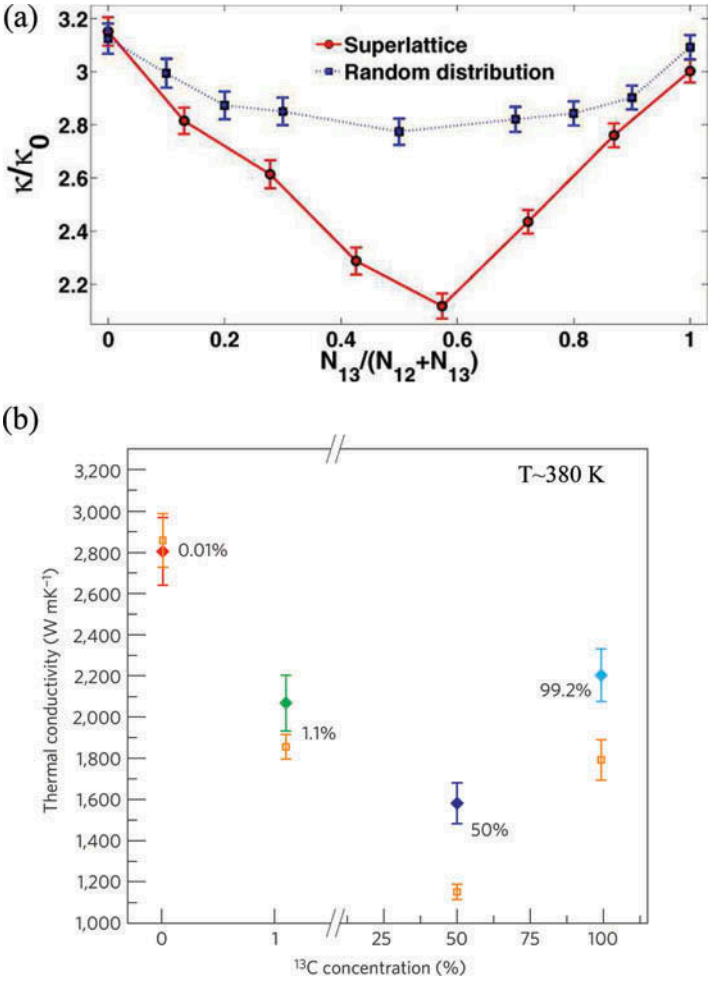

Figure 6 (a) κ of GNR as a function of isotopic composition (^{12}C and ^{13}C) predicted from NEMD simulations. Blue squares: randomly distributed isotopes. Red circles: isotopes arranged as a superlattice. (b) κ of graphene as a function of isotopic composition at ~380 K. Solid diamonds: experiment results. Open squares: GK-MD results. Panels reproduced (a) Hu et al. [97], © AIP Publishing, LLC. Reproduced by permission of AIP Publishing, LLC, and (b) Chen et al. [96], © Nature Publishing Group. Reproduced by permission of Nature Publishing Group. Permission to reuse must be obtained from the rightsholder.

[99, 100], and how to transform such high-κ materials into low-κ ones as required by thermoelectrics is challenging but attractive [101, 102].

MD simulations have been conducted to study the isotopic effect in graphene and GNRs [96, 97, 103–105]. A general trend of the predicted κ versus isotopic composition is a U-shaped curve like the one shown in Figure 6a, where κ is higher for isotopically purer compositions and lower in between. Figure 6a also indicates that by arranging the isotopes in a periodic manner—that is, superlattice—κ may be reduced below the random isotope limit. The experiment by Chen et al. [96], in which the κ of isotopically modified graphene for ^{13}C concentrations of 0.01%, 1.1% (natural abundance), 50%, and 99.2% was measured, is the first time that the isotopic effets on thermal transport in graphene have been

experimentally studied (see Figure 6b). In particular, at ~320 K, κ of isotopically purified samples (0.01% ^{13}C) is higher than 4,000 W/m-K, much higher than that (~2,600 W/m-K) of the samples with natural abundance (1.1% ^{13}C). The authors also conducted GK-MD simulations to calculate the κs for different isotropic compositions, which agree reasonably well with experimental values, as can be seen in Figure 6b.

The largely scattered values of measured κ of graphene have been attributed to the uncontrolled formation of defects in experiments. Fthenakis and Tomanek [98] studied graphene containing isotopes and vacancies. κ was found to be hardly affected by <10% ^{13}C isotope doping at RT when phonon–phonon scattering dominates. In contrast, di-vacancy defects can reduce κ by >50% in a wide temperature range even with <1% concentration.

Thermal transport across grain boundaries, another type of defect in crystal structures, has also been studied [106–108]. The thermal boundary conductance, G_I, computed from MD simulations is on the order of 10 GW/m^2-K, whereas the NEGF predicted results are on the order of 1 GW/m^2-K. The large inconsistency should be due to methodological reasons—on one hand, MD tends to overestimate G_I because it uses the classical limit of heat capacity, which is higher than the quantum one for $T < \Theta_D$; on the other hand, inelastic phonon scattering can promote interfacial thermal transport, which can be captured by MD but not NEGF.

INTERFACIAL THERMAL TRANSPORT

Interfacial thermal resistance (R_I) between graphene and other materials has been extensively studied. R_I is defined as $R_I = 1/G_I = A\Delta T/J$, where A is the contact area, ΔT is the temperature drop at the interface, and J is the heat current. In some applications, graphene is an active component of the device; for example, graphene transistors. In other cases, graphene is used as a thermal interface material to fill the air gaps at interfaces. In both scenarios, a high κ and low R_I are desired. Graphene may be vertically (end-contact) or horizontally (side-contact) aligned with the substrate depending on the application, and the heat transfer mechanism should be different due to the different ways of phonon–phonon coupling across the interface.

Horizontal Alignment of Graphene on Substrate

For thermal transport across graphene/dielectric interface, Ong et al. [109] studied the thermal transport across the graphene–silica interface with GK-MD simulations and the NEGF method, where the coupling between graphene phonons and substrate surface phonons was believed to be the dominant mechanism for interfacial thermal transport. As shown in Figure 7a, NEGF calculation suggests that most of the heat transfer is aided by out-of-plane phonons in graphene, whereas in-plane ones are much less effective in transporting energy across the interface. Ong et al. also conducted SED analysis for graphene, which showed that ZA phonons with moderate wave vectors couples with the substrate most strongly. They attributed such behavior to flexural resonance as described by Persson and Ueba [110], who proposed that G_I should be dominated by the coupling between the flexural mode in graphene and the Rayleigh mode at the substrate surface.

As for graphene–metal interfaces, DFT calculations have revealed that the bonding between graphene and various metals can be categorized into two types—chemisorption and physisorption—of which the former is characterized by strong bonding that opens a

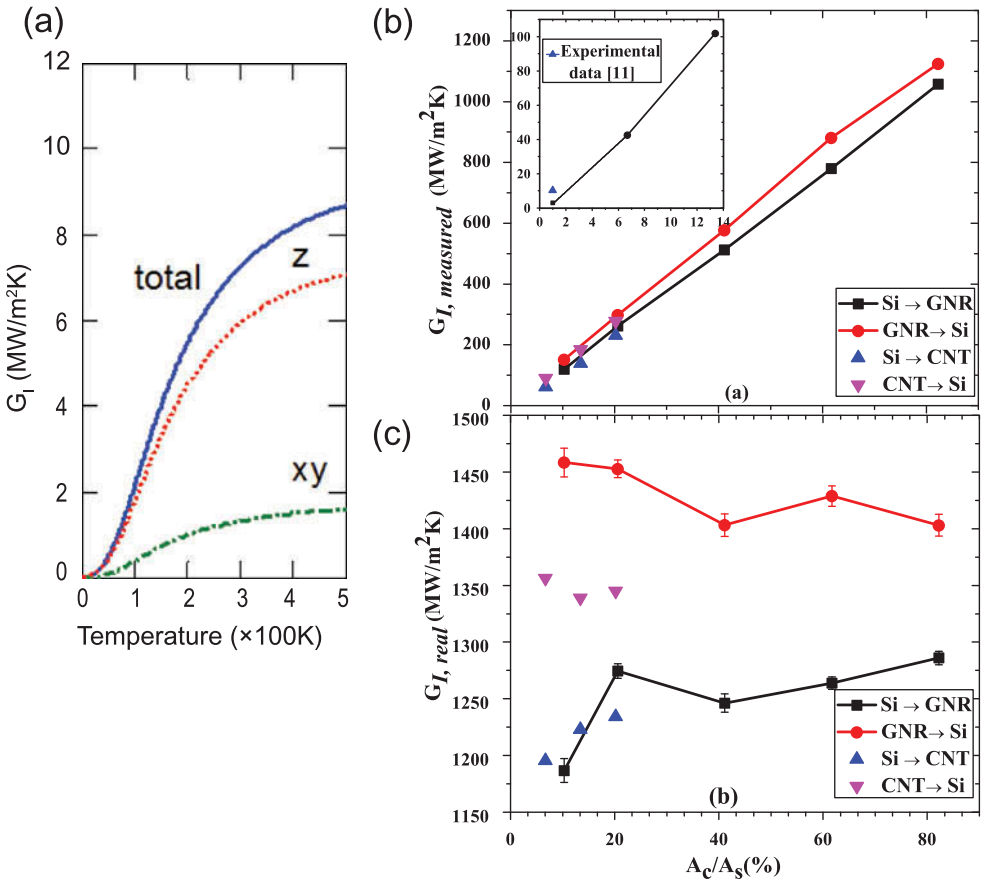

Figure 7 (a) G_I resolved by polarization; that is, in-plane (xy) and out-of-plane (z), as a function of T [109]. (b) and (c) $G_{I,measured}$ and $G_{I,real}$ as a function of filling fraction. Panels reproduced (b) and (c) Vallabhaneni et al. [111], © AIP Publishing, LLC. Reproduced by permission of AIP Publishing, LLC. Permission to reuse must be obtained from the rightsholder.

band gap in graphene, whereas the latter is weak such that the Dirac-cone energy band of graphene is preserved [112]. Mao et al. calculated R_I of the side-contact interface between graphene and different metals (Ni, Cu, Au, Pd) using the first-principles NEGF method [113]. The RT R_I of those interfaces was found to vary by one order of magnitude but not to monotonically decrease with increasing interfacial bonding strength.

Vertical Alignment of Graphene on Substrate

For vertical graphene on substrates, the computationally predicted R_I is usually orders of magnitude lower than experimental data, and the incomplete filling of graphene or CNTs at the interface was believed to account for most of the discrepancies [114, 115]. A parameter often referred to as filling fraction or volume fraction is defined as the ratio of the contact area to the surface area of the substrate. The contact area is $w\delta$ and $\pi d\delta$ for graphene and CNT in end-contact with substrate, respectively. The real G_I is usually computed from the measured values by $G_{I,real} = G_{I,measured}/\text{filling fraction}$, but it is not known whether such linear dependence still holds when there is considerable interlayer coupling between

graphene flakes at high filling fractions. Vallabhaneni et al. [111] used NEMD simulations to study the filling fraction dependence of G_I for graphene–Si interfaces. The Tersoff potential for covalent C-Si bonding was used in their simulations. $G_{I,real}$ was found to increase linearly with the filling fraction, indicating a negligible effect of interlayer coupling on G_I. They also computed the effective G_I considering the highest possible filling fraction for graphene in end-contact with Si, and the values are in the range of 0.2–1.2 GW/m^2-K, which are still orders of magnitude higher than experimental values [114–116], suggesting much room for improvement in graphene- and CNT-based thermal management solely by increasing the filling fraction.

In graphene-based nanocomposites, graphene flakes are embedded in an organic matrix so that both the horizontal and vertical alignment of graphene exists in such structures. Graphene flakes may improve the alignment of organic molecules adjacent to their surfaces, which can affect the organic phase thermal conductivity. In addition, the edges of graphene flakes are usually passivated with hydrogen or oxygen atoms and such edge passivation was shown to affect the thermal conductance between graphene flakes [117]. Hu et al. studied graphene embedded in an organic matrix with MD simulations and observed that graphene can enhance the κ of nanocomposites significantly [40, 118].

3D Architectures

Pillared graphene architectures (PGA) [119, 120] have been proposed for thermal management applications, where the PGA is built in such a way that phonons can transport easily in the two dimensions of the graphene plane and can also readily propagate in the third dimension, which is parallel to the vertically aligned CNTs. This design may be a solution to the practical problem of using graphene and CNTs as TIMs; that is, the very low κ in the directions perpendicular to the graphene plane or CNTs axis, which could seriously degrade heat dissipation performance when they are misaligned. Varshney et al. claimed that phonon scatterings at the CNT–graphene junctions dominate the overall thermal resistance of PGA based on NEMD simulations [119], and phonon transmission across individual CNT–graphene junction was modeled with the phonon WP method by Lee et al. [120].

Beyond Phonon–Phonon Coupling

In the above, the interfacial thermal transport is contributed solely by phonon–phonon coupling across the interface between graphene and other materials. It should be noted that thermal transport across the interface between graphene and metals depends not only on phonon properties but also on electron properties as well as electron–phonon coupling [121, 122]. In addition, surface phonon–polariton scattering has also been revealed to account for a significant part of heat dissipation from graphene to polar substrates; for example, SiO_2 and hexagonal boron nitride (h-BN) [123]. Rigorous atomistic modeling of the above processes would benefit the thermal management of graphene-based devices but it is still lacking.

NONLINEAR THERMAL TRANSPORT

In the above sections, we have discussed linear thermal transport in graphene-related structures, which is characterized by a specific κ, G, or R. Nonlinear thermal transport

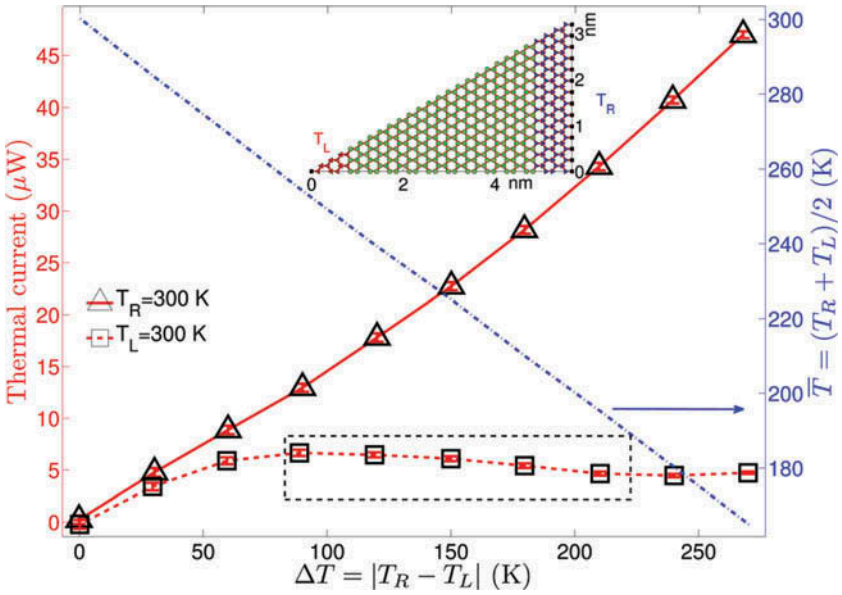

Figure 8 Heat current (triangles denote heat flow in the decreasing width direction and vice versa for rectangles) and average temperature vs. temperature difference ΔT for the triangular GNR shown in the inset. The dashed box indicates where NDTR occurs. Figure reproduced from Hu et al. [124], © AIP Publishing, LLC. Reproduced by permission of AIP Publishing, LLC. Permission to reuse must be obtained from the rightsholder.

properties, which open the possiblity of various other applications, will be discussed in this section.

Thermal rectification (TR) is a phenomenon in which heat flow is directional dependent; that is, heat current changes in magnitude as the temperature bias is reversed. Figure 8 shows the NEMD simulation results for a triangular GNR [124], and TR exists noting that the heat current is different when the temperature bias ΔT is reversed. A dimensionless parameter, the thermal rectification ratio (η), is usually used to quantify TR, which is defined as

$$\eta = \frac{\kappa_{forward} - \kappa_{reverse}}{\kappa_{reverse}} \times 100\%, \tag{8}$$

where the subscripts *forward* and *reverse* denote the two opposite directions pointing from one end to the other. TR is a thermal analogue of the electrical diode where the current-carrying ability of the device under forward bias is much higher than under reverse bias. A perfect thermal rectifier would be one that is highly thermally conductive in one direction while insulating in the other, and it is expected to work as a promising thermal management component of electronics as chip size continues decreasing or as a basic component for thermal computing [125, 126].

Although the earliest proposal of TR in bulk 3D materials dates back to the 1930s [127], only since the middle of the last decade has extensive attention been paid to CNT and graphene-based systems [24, 26, 93, 111, 126, 128–137]. To date, proposed thermal rectifiers include physically/chemically functionalized GNRs and CNTs or heterojunctions composed of GNR/CNT and other materials. In all of the existing designs,

a spatial asymmetry in geometry, defect concentration, isotope concentration, or an interface between two materials is necessary for TR to occur, and η can be tuned by adjusting the magnitude of such asymmetries [26, 128, 129]. Many other factors were also found to affect η; for instance, high T usually reduces η, high ΔT enhances η, and η decreases with the length of the system to zero in the bulk limit[133] or saturates when the length increases [129].

Although that many schemes are possible to apply to make thermal rectifiers, the fact that η can be reduced by the presence of lattice disorders such as edge roughness [138] and defects [133, 138] may make it difficult for the observation of significant TR experimentally, considering that η may not be high enough to prevail measurement uncertainties.

Negative differential thermal resistance (NDTR) is another thermal analog to nonlinear electrical transport phenomenon. In a linear thermal transport regime, the heat current J is proportional to the applied bias ΔT. In contrast, NDTR describes a phenomenon in which J decreases with increasing ΔT. Hu et al. observed NDTR in rectangular and triangular GNRs in their NEMD simulations [124], as shown in Figure 8. The onset ΔT was found to depend on the average temperature of the GNR, which provides full analogy between such thermal device with electrical transistors, where the average T works like the gate voltage, and the temperature bias ΔT works like the electrical bias between the source and drain in transistors. Hu et al. attributed the NDTR to the temperature dependence of κ, which modifies the average κ so much at large ΔT that the J-ΔT trend is reversed. In contrast, Ai et al. [139] attributed the onset of NDTR as the increasing thermal boundary resistance between the GNR and the heat baths, which implies that NDTR is an extrinsic mechanism rather than an intrinsic one due to the change in κ of GNR. More recently, Ai et al. explored the NDTR phenomenon in SWCNTs, and the most notable observation is the disappearing NDTR in longer CNTs, which implies that the real application of such nonlinear property requires nanosized structures.

CONCLUSION AND OUTLOOK

In this review, we have discussed recent numerical modeling studies on thermal transport in graphene-related structures. Graphene possesses many unique properties due to the 2D structure. A high ZA branch contribution to κ in suspended graphene has been reported, which was attributed to the unique selection rule hindering the scattering of ZA phonons. This endows graphene with extremely high κ as well as its sensitivity to substrate coupling. The κ of MLG was found to decrease with increasing number of layers until it converges to the graphite limit. Mechanisms such as curvature effect, edge effect, mode quantization, etc., have been used to explain the transition from 2D thermal transport in bulk graphene to the quasi-1D transport in CNTs and GNRs. Isotopes, impurities, and defects can reduce the κ of graphene by different degrees. Interfacial thermal transport between graphene and other materials has also been discussed. For graphene horizontally supported on a substrate, heat is mostly transferred via the coupling between flexural phonons in graphene and the surface phonons of the substrate, which is a unique feature of 2D materials. The filling fraction was shown to limit the effective thermal boundary conductance of vertically aligned graphene on substrate. Nonlinear thermal transport phenomena such as TR and NDTR have been explored extensively, which could possibly be used in thermal signal manipulation or thermal management in the future benefiting from the advancement in nanofabrication techniques.

Numerical modeling has played an important role in advancing the understanding of the real world and, considering the rapid advance in computational power of supercomputers and computing algorithms, we expect numerical studies to provide faster and more effective guidance to experiments in the future. Direct atomistic simulations of thermal transport in the diffusive regime for many materials including graphene and CNTs may be possible and thereby problems currently puzzling scientists—for instance, the size dependence of the κ of low-dimensional materials—can be solved. The 2013 Nobel Prize in Chemistry was awarded to the development of multiscale models using both classical and quantum physics [140], and similar efforts have also been going on in the heat transfer community. The lack of proper quantum treatment of phonon properties in MD makes the interpretation of sub-Θ_D simulation results tricky, and more accurate quantum correction methods are needed. Although NEGF and BTE can include quantum effects in the heat capacity, the difficulty in accurately dealing with higher-order anharmonic phonon scatterings hinders their broad application at high temperatures, and advances in this area can significantly enhance their capability for thermal transport prediction. Another limitation to classical MD simulations is their great dependence on EIPs, which are mostly developed at ground-state conditions and may not be good for excited states arising from thermal (finite T), optical (e.g., laser radiation), or electrical excitations. Moreover, the simplified forms of EIPs cannot fully describe the complex interatomic interactions in the real world. The *ab initio* MD method [44] computes the forces acting on the nuclei from electronic structures "on-the-fly", and thereby it is free from the need of EIPs. However, the high computational cost restricts existing *ab initio* MD-based thermal modelings to systems of $\sim$100 atoms for several femtoseconds to several picoseconds [46, 141, 142], which is inadequate for graphene due to the high λ and τ. All in all, we would expect more thermal modeling using such first-principles methods in the future.

FUNDING

The authors are grateful for the support from the Air Force Office of Scientific Research (AFOSR), the National Science Foundation, and the Purdue Cooling Technologies Research Center, a NSF University/Industry Cooperation Research Center.

REFERENCES

1. K.S. Novoselov, A.K. Geim, S. Morozov, D. Jiang, Y. Zhang, S. Dubonos, I. Grigorieva, and A. Firsov, Electric Field Effect in Atomically Thin Carbon Films, *Science*, Vol. 306, No. 5696, pp. 666–669, 2004.
2. Y. Zhang, Y.-W. Tan, H.L. Stormer, and P. Kim, Experimental Observation of the Quantum Hall Effect and Berry's Phase in Graphene, *Nature*, Vol. 438, No. 7065, pp. 201–204, 2005.
3. J.-C. Charlier, X. Blase, and S. Roche, Electronic and Transport Properties of Nanotubes, *Reviews of Modern Physics*, Vol. 79, pp. 677–732, 2007.
4. R. Nair, P. Blake, A. Grigorenko, K. Novoselov, T. Booth, T. Stauber, N. Peres, and A. Geim, Fine Structure Constant Defines Visual Transparency of Graphene, *Science*, Vol. 320, No. 5881, pp. 1308–1308, 2008.
5. Z. Wu, Z. Chen, X. Du, J.M. Logan, J. Sippel, M. Nikolou, K. Kamaras, J.R. Reynolds, D.B. Tanner, A.F. Hebard, and A.G. Rinzler, Transparent, Conductive carbon Nanotube Films, *Science*, Vol. 305, No. 5688, pp. 1273–1276, 2004.
6. S. Berber, Y.-K. Kwon, and D. Tománek, Unusually High Thermal Conductivity of Carbon Nanotubes, *Physical Review Letters*, Vol. 84, pp. 4613–4616, 2000.

7. A.A. Balandin, S. Ghosh, W. Bao, I. Calizo, D. Teweldebrhan, F. Miao, and C.N. Lau, Superior Thermal Conductivity of Single-Layer Graphene, *Nano Letters*, Vol. 8, No. 3, pp. 902–907, 2008.
8. C. Lee, X. Wei, J.W. Kysar, and J. Hone, Measurement of the Elastic Properties and Intrinsic Strength of Monolayer Graphene, *Science*, Vol. 321, No. 5887, pp. 385–388, 2008.
9. M.-F. Yu, O. Lourie, M.J. Dyer, K. Moloni, T.F. Kelly, and R.S. Ruoff, Strength and Breaking Mechanism of Multiwalled Carbon Nanotubes under Tensile Load, *Science*, Vol. 287, No. 5453, pp. 637–640, 2000.
10. Y.-W. Son, M.L. Cohen, and S.G. Louie, Energy Gaps in Graphene Nanoribbons, *Physical Review Letters*, Vol. 97, No. 21, p. 216803, 2006.
11. Y.-W. Son, M.L. Cohen, and S.G. Louie, Half-Metallic Graphene Nanoribbons, *Nature*, Vol. 444, No. 7117, pp. 347–349, 2006.
12. O. Dubay, and G. Kresse, Accurate Density Functional Calculations for the Phonon Dispersion Relations of Graphite Layer and Carbon Nanotubes, *Physical Review B*, Vol. 67, p. 035401, 2003.
13. C. Oshima, T. Aizawa, R. Souda, Y. Ishizawa, and Y. Sumiyoshi, Surface Phonon Dispersion Curves of Graphite (0001) over the Entire Energy Region, *Solid State Communications*, Vol. 65, No. 12, pp. 1601–1604, 1988.
14. S. Siebentritt, R. Pues, K.-H. Rieder, and A.M. Shikin, Surface Phonon Dispersion in Graphite and in a Lanthanum Graphite Intercalation Compound, *Physical Review B*, Vol. 55, pp. 7927–7934, 1997.
15. L. Lindsay, D.A. Broido, and N. Mingo, Flexural Phonons and Thermal Transport in Graphene, *Physical Review B*, Vol. 82, p. 115427, 2010.
16. L. Lindsay, D.A. Broido, and N. Mingo, Diameter Dependence of Carbon Nanotube Thermal Conductivity and Extension to the Graphene Limit, *Physical Review B*, Vol. 82, p. 161402, 2010.
17. S. Ghosh, W. Bao, D.L. Nika, S. Subrina, E.P. Pokatilov, C.N. Lau, and A.A. Balandin, Dimensional Crossover of Thermal Transport in Few-Layer Graphene, *Nature Materials*, Vol. 9, No. 7, pp. 555–558, 2010.
18. S. Ghosh, I. Calizo, D. Teweldebrhan, E.P. Pokatilov, D.L. Nika, A.A. Balandin, W. Bao, F. Miao, and C.N. Lau, Extremely High Thermal Conductivity of Graphene: Prospects for Thermal Management Applications in Nanoelectronic Circuits, *Applied Physics Letters*, Vol. 92, No. 15, p. 151911, 2008.
19. S. Chen, A.L. Moore, W. Cai, J.W. Suk, J. An, C. Mishra, C. Amos, C.W. Magnuson, J. Kang, L. Shi, and R.S. Ruoff, Raman Measurements of Thermal Transport in Suspended Monolayer Graphene of Variable Sizes in Vacuum and Gaseous Environments, *ACS Nano*, Vol. 5, No. 1, pp. 321–328, 2010.
20. C. Faugeras, B. Faugeras, M. Orlita, M. Potemski, R.R. Nair, and A. Geim, Thermal Conductivity of Graphene in Corbino Membrane Geometry, *Acs Nano*, Vol. 4, No. 4, pp. 1889–1892, 2010.
21. J.H. Seol, I. Jo, A.L. Moore, L. Lindsay, Z.H. Aitken, M.T. Pettes, X. Li, Z. Yao, R. Huang, D. Broido, N. Mingo, and L. Shi, Two-Dimensional Phonon Transport in Supported Graphene, *Science*, Vol. 328, No. 5975, pp. 213–216, 2010.
22. W. Cai, A.L. Moore, Y. Zhu, X. Li, S. Chen, L. Shi, and R.S. Ruoff, Thermal Transport in Suspended and Supported Monolayer Graphene Grown by Chemical Vapor Deposition, *Nano Letters*, Vol. 10, No. 5, pp. 1645–1651, 2010.
23. M.M. Sadeghi, M.T. Pettes, and L. Shi, Thermal Transport in Graphene, *Solid State Communications*, Vol. 152, No. 15, pp. 1321–1330, 2012.
24. C. Chang, D. Okawa, A. Majumdar, and A. Zettl, Solid-State Thermal Rectifier, *Science*, Vol. 314, No. 5802, pp. 1121–1124, 2006.
25. L. Lindsay, D. Broido, and N. Mingo, Flexural Phonons and Thermal Transport in Multilayer Graphene and Graphite, *Physical Review B*, Vol. 83, No. 23, p. 235428, 2011.

26. M. Alaghemandi, E. Algaer, M.C. Böhm, and F. Müller-Plathe, The Thermal Conductivity and Thermal Rectification of Carbon Nanotubes Studied Using Reverse Non-Equilibrium Molecular Dynamics Simulations, *Nanotechnology*, Vol. 20, No. 11, p. 115704, 2009.
27. B. Qiu, Y. Wang, Q. Zhao, and X. Ruan, The Effects of Diameter and Chirality on the Thermal Transport in Free-Standing and Supported Carbon-Nanotubes, *Applied Physics Letters*, Vol. 100, No. 23, p. 233105, 2012.
28. M.-H. Bae, Z. Li, Z. Aksamija, P.N. Martin, F. Xiong, Z.-Y. Ong, I. Knezevic, and E. Pop, Ballistic to Diffusive Crossover of Heat Flow in Graphene Ribbons, *Nature Communications*, Vol. 4, pp. 1734–1741, 2013.
29. Z.W. Tan, J.-S. Wang, and C.K. Gan, First-Principles Study of Heat Transport Properties of Graphene Nanoribbons, *Nano Letters*, Vol. 11, No. 1, pp. 214–219, 2011.
30. Y. Wang, B. Qiu, and X. Ruan, Edge Effect on Thermal Transport in Graphene Nanoribbons: A Phonon Localization Mechanism beyond Edge Roughness Scattering, *Applied Physics Letters*, Vol. 101, No. 1, p. 013101, 2012.
31. J. Haskins, A. Knac, C. Sevik, H. Sevincli, G. Cuniberti, and T. Çağin, Control of Thermal and Electronic Transport in Defect-Engineered Graphene Nanoribbons, *ACS Nano*, Vol. 5, No. 5, pp. 3779–3787, 2011.
32. Z. Aksamija, and I. Knezevic, Lattice Thermal Conductivity of Graphene Nanoribbons: Anisotropy and Edge Roughness Scattering, *Applied Physics Letters*, Vol. 98, No. 14, p. 141919, 2011.
33. D.V. Kosynkin, A.L. Higginbotham, A. Sinitskii, J.R. Lomeda, A. Dimiev, B.K. Price, and J.M. Tour, Longitudinal Unzipping of Carbon Nanotubes to Form Graphene Nanoribbons, *Nature*, Vol. 458, No. 7240, pp. 872–876, 2009.
34. Y. Jiang, H. Li, Y. Li, H. Yu, K.M. Liew, Y. He, and X. Liu, Helical Encapsulation of Graphene Nanoribbon into Carbon Nanotube, *ACS Nano*, Vol. 5, No. 3, pp. 2126–2133, 2011.
35. A. Casher, and J.L. Lebowitz, Heat Flow in Regular and Disordered Harmonic Chains, *Journal of Mathematical Physics*, Vol. 12, No. 8, pp. 1701–1711, 1971.
36. R.J. Rubin, and W.L. Greer, Abnormal Lattice Thermal Conductivity of a One-Dimensional, Harmonic, Isotopically Disordered Crystal, *Journal of Mathematical Physics*, Vol. 12, No. 8, pp. 1686–1701, 1971.
37. L.W. Lee, and A. Dhar, Heat Conduction in a Two-Dimensional Harmonic Crystal with Disorder, *Physical Review Letters*, Vol. 95, p. 094302, 2005.
38. P.K. Schelling, S.R. Phillpot, and P. Keblinski, Comparison of Atomic-Level Simulation Methods for Computing Thermal Conductivity, *Physical Review B*, Vol. 65, p. 144306, 2002.
39. F. Müller-Plathe, A Simple Nonequilibrium Molecular Dynamics Method for Calculating the Thermal Conductivity, *The Journal of Chemical Physics*, Vol. 106, No. 14, pp. 6082–6085, 1997.
40. L. Hu, T. Desai, and P. Keblinski, Determination of Interfacial Thermal Resistance at the Nanoscale, *Physical Review B*, Vol. 83, No. 19, p. 195423, 2011.
41. P. Schelling, S. Phillpot, and P. Keblinski, Phonon Wave-Packet Dynamics at Semiconductor Interfaces by Molecular-Dynamics Simulation, *Applied Physics Letters*, Vol. 80, No. 14, pp. 2484–2486, 2002.
42. A.J.H. McGaughey, and M. Kaviany, Quantitative Validation of the Boltzmann Transport Equation Phonon Thermal Conductivity Model under the Single-Mode Relaxation Time Approximation, *Physical Review B*, Vol. 69, p. 094303, 2004.
43. A.S. Henry, and G. Chen, Spectral Phonon Transport Properties of Silicon Based on Molecular Dynamics Simulations and Lattice Dynamics, *Journal of Computational and Theoretical Nanoscience*, Vol. 5, No. 2, pp. 141–152, 2008.
44. R. Car, and M. Parrinello, Unified Approach for Molecular Dynamics and Density-Functional Theory, *Physical Review Letters*, Vol. 55, pp. 2471–2474, 1985.
45. M. Pozzo, C. Davies, D. Gubbins, and D. Alfè, Thermal and Electrical Conductivity of Iron at Earth's Core Conditions, *Nature*, Vol. 485, No. 7398, pp. 355–358, 2012.

46. T. Gibbons, By. Kang, S. Estreicher, and C. Carbogno, Thermal Conductivity of Si Nanostructures Containing Defects: Methodology, Isotope Effects, and Phonon Trapping, *Physical Review B*, Vol. 84, No. 3, p. 035317, 2011.
47. V.K. Tewary, and B. Yang, Singular Behavior of the Debye-Waller Factor of Graphene, *Physical Review B*, Vol. 79, p. 125416, 2009.
48. C. Oligschleger, and J. Schön, Simulation of Thermal Conductivity and Heat Transport in Solids, *Physical Review B*, Vol. 59, No. 6, pp. 4125–4133, 1999.
49. M. Kaviany, *Heat Transfer Physics*, Cambridge University Press, Cambridge, UK, 2008.
50. A. McGaughey, and M. Kaviany, Thermal Conductivity Decomposition and Analysis Using Molecular Dynamics Simulations. Part I. Lennard-Jones Argon, *International Journal of Heat and Mass Transfer*, Vol. 47, No. 8, pp. 1783–1798, 2004.
51. H. Kaburaki, J. Li, and S. Yip, Thermal Conductivity of Solid Argon by Classical Molecular Dynamics, *Materials Research Society Symposium Proceedings*, in eds. V. Bulatov, N.M. Ghoniem, T. Kaxiras, R. Phillips, T. Diaz de la Rubia, Vol. 538, Cambridge University Press, New York, pp. 503–508, 1999.
52. P.C. Howell, Comparison of Molecular Dynamics Methods and Interatomic Potentials for Calculating the Thermal Conductivity of Silicon, *The Journal of Chemical Physics*, Vol. 137, No. 22, p. 224111, 2012.
53. K. Esfarjani, G. Chen, and H.T. Stokes, Heat Transport in Silicon from First-Principles Calculations, *Physical Review B*, Vol. 84, No. 8, p. 085204, 2011.
54. A. McGaughey, Predicting Phonon Properties from Equilibrium Molecular Dynamics Simulations, *Annual Review of Heat Transfer*, Vol. 17, to appear.
55. A.J.C. Ladd, B. Moran, and W.G. Hoover, Lattice Thermal Conductivity: A Comparison of Molecular Dynamics and Anharmonic Lattice Dynamics, *Physical Review B*, Vol. 34, pp. 5058–5064, 1986.
56. N. de Koker, Thermal Conductivity of MgO Periclase from Equilibrium First Principles Molecular Dynamics, *Physical Review Letters*, Vol. 103, p. 125902, 2009.
57. W. Zhang, T.S. Fisher, and N. Mingo, The Atomistic Green's Function Method: An Efficient Simulation Approach for Nanoscale Phonon Transport, *Numerical Heat Transfer, Part B: Fundamentals*, Vol. 51, No. 4, pp. 333–349, 2007.
58. J.-S. Wang, B.K. Agarwalla, H. Li, and J. Thingna, Nonequilibrium Green's Function Method for Quantum Thermal Transport, *Frontiers of Physics*, pp. 1–24, 2013.
59. J. Lan, J.-S. Wang, C.K. Gan, and S.K. Chin, Edge Effects on Quantum Thermal Transport in Graphene Nanoribbons: Tight-Binding Calculations, *Physical Review B*, Vol. 79, p. 115401, 2009.
60. J. Wang, L. Li, and J.-S. Wang, Tuning Thermal Transport in Nanotubes with Topological Defects, *Applied Physics Letters*, Vol. 99, No. 9, p. 091905, 2011.
61. N. Mingo, Anharmonic Phonon Flow through Molecular-Sized Junctions, *Physical Review B*, Vol. 74, p. 125402, 2006.
62. G.P. Srivastava, *The Physics of Phonons*, Taylor & Francis Group, 1990.
63. M. Omini, and A. Sparavigna, An Iterative Approach to the Phonon Boltzmann Equation in the Theory of Thermal Conductivity, *Physica B: Condensed Matter*, Vol. 212, No. 2, pp. 101–112, 1995.
64. L. Lindsay, D. Broido, and N. Mingo, Lattice Thermal Conductivity of Single-Walled Carbon Nanotubes: Beyond the Relaxation Time Approximation and Phonon-Phonon Scattering Selection Rules, *Physical Review B*, Vol. 80, No. 12, p. 125407, 2009.
65. J. Tersoff, New Empirical Approach for the Structure and Energy of Covalent Systems, *Physical Review B*, Vol. 37, No. 12, pp. 6991–7000, 1988.
66. J. Tersoff, Modeling Solid-State Chemistry: Interatomic Potentials for Multicomponent Systems, *Physical Review B*, Vol. 39, No. 8, pp. 5566–5568, 1989.

67. S.J. Stuart, A.B. Tutein, and J.A. Harrison, A Reactive Potential for Hydrocarbons with Intermolecular Interactions, *The Journal of Chemical Physics*, Vol. 112, No. 14, pp. 6472–6486, 2000.
68. D.W. Brenner, O.A. Shenderova, J.A. Harrison, S.J. Stuart, B. Ni, and S.B. Sinnott, A Second-Generation Reactive Empirical Bond Order (Rebo) Potential Energy Expression for Hydrocarbons, *Journal of Physics: Condensed Matter*, Vol. 14, No. 4, pp. 783–802, 2002.
69. L. Lindsay, and D.A. Broido, Optimized Tersoff and Brenner Empirical Potential Parameters for Lattice Dynamics and Phonon Thermal Transport in Carbon Nanotubes and Graphene, *Physical Review B*, Vol. 81, p. 205441, 2010.
70. R. Nicklow, N. Wakabayashi, and H.G. Smith, Lattice Dynamics of Pyrolytic Graphite, *Physical Review B*, Vol. 5, pp. 4951–4962, 1972.
71. L.A. Girifalco, M. Hodak, and R.S. Lee, Carbon Nanotubes, Buckyballs, Ropes, and a Universal Graphitic Potential, *Physical Review B*, Vol. 62, pp. 13104–13110, 2000.
72. M.H. Khadem, and A.P. Wemhoff, Molecular Dynamics Predictions of the Influence of Graphite Stacking Arrangement on the Thermal Conductivity Tensor, *Chemical Physics Letters*, Vol. 574, pp. 78–82, 2013.
73. J.A. Thomas, R.M. Iutzi, and A.J.H. McGaughey, Thermal Conductivity and Phonon Transport in Empty and Water-Filled Carbon Nanotubes, *Physical Review B*, Vol. 81, p. 045413, 2010.
74. W.J. Evans, L. Hu, and P. Keblinski, Thermal Conductivity of Graphene Ribbons from Equilibrium Molecular Dynamics: Effect of Ribbon Width, Edge Roughness, and Hydrogen Termination, *Applied Physics Letters*, Vol. 96, No. 20, p. 203112, 2010.
75. B. Qiu, and X. Ruan, Mechanism of Thermal Conductivity Reduction from Suspended to Supported Graphene: a Quantitative Spectral Analysis of Phonon Scattering, ASME 2011 International Mechanical Engineering Congress and Exposition, 11–17 November, Denver, CO, pp. 303–313.
76. D.L. Nika, E.P. Pokatilov, A.S. Askerov, and A.A. Balandin, Phonon thermal conduction in graphene: Role of umklapp and edge roughness scattering, *Phys. Rev. B*, Vol. 79, p. 155413, 2009.
77. D. Singh, J.Y. Murthy, and T.S. Fisher, Spectral Phonon Conduction and Dominant Scattering Pathways in Graphene, *Journal of Applied Physics*, Vol. 110, No. 9, p. 094312, 2011.
78. B. Qiu, and X. Ruan, Reduction of Spectral Phonon Relaxation Times from Suspended to Supported Graphene, *Applied Physics Letters*, Vol. 100, No. 19, p. 193101, 2012.
79. L. Chen, and S. Kumar, Thermal Transport in Graphene Supported on Copper, *Journal of Applied Physics*, Vol. 112, No. 4, p. 043502, 2012.
80. A. Alofi, and G.P. Srivastava, Phonon Conductivity in Graphene, *Journal of Applied Physics*, Vol. 112, No. 1, p. 013517, 2012.
81. Z. Guo, D. Zhang, and X.-G. Gong, Thermal Conductivity of Graphene Nanoribbons, *Applied Physics Letters*, Vol. 95, No. 16, p. 163103, 2009.
82. J. Chen, G. Zhang, and B. Li, Substrate Coupling Suppresses Size Dependence of Thermal Conductivity in Supported Graphene, *Nanoscale*, Vol. 5, No. 2, pp. 532–536, 2012.
83. C. Yu, and G. Zhang, Impacts of Length and Geometry Deformation on Thermal Conductivity of Graphene Nanoribbons, *Journal of Applied Physics*, Vol. 113, No. 4, p. 044306, 2013.
84. A. Selezenev, A.Y. Aleinikov, N. Ganchuk, S. Ganchuk, R. Jones, and J. Zimmerman, Molecular Dynamics Calculation of the Thermal Conductivity Coefficient of Single-Layer and Multilayer Graphene Sheets, *Physics of the Solid State*, Vol. 55, No. 4, pp. 889–894, 2013.
85. Z.-Y. Ong, and E. Pop, Effect of Substrate Modes on Thermal Transport in Supported Graphene, *Physical Review B*, Vol. 84, No. 7, p. 075471, 2011.
86. Z. Wei, Z. Ni, K. Bi, M. Chen, and Y. Chen, In-Plane Lattice Thermal Conductivities of Multilayer Graphene Films, *Carbon*, Vol. 49, No. 8, pp. 2653–2658, 2011.
87. P. Klemens, Theory of the A-Plane Thermal Conductivity of Graphite, *Journal of Wide Bandgap Materials*, Vol. 7, No. 4, pp. 332–339, 2000.

88. W.-R. Zhong, M.-P. Zhang, B.-Q. Ai, and D.-Q. Zheng, Chirality and Thickness-Dependent Thermal Conductivity of Few-Layer Graphene: A Molecular Dynamics Study, *Applied Physics Letters*, Vol. 98, No. 11, p. 113107, 2011.
89. M.H. Khadem, and A.P. Wemhoff, Thermal Conductivity Predictions of Herringbone Graphite Nanofibers Using Molecular Dynamics Simulations, *The Journal of Chemical Physics*, Vol. 138, No. 8, p. 084708, 2013.
90. D. Singh, J.Y. Murthy, and T.S. Fisher, Mechanism of Thermal Conductivity Reduction in Few-Layer Graphene, *Journal of Applied Physics*, Vol. 110, No. 4, p. 044317, 2011.
91. G. Zhang, and B. Li, Thermal Conductivity of Nanotubes Revisited: Effects of Chirality, Isotope Impurity, Tube Length, and Temperature, *The Journal of Chemical Physics*, Vol. 123, No. 11, p. 114714, 2005.
92. J. Shiomi, and S. Maruyama, Molecular Dynamics of Diffusive-Ballistic Heat Conduction in Single-Walled Carbon Nanotubes, *Japanese Journal of Applied Physics-Part 1 Regular Papers and Short Notes*, Vol. 47, No. 4, pp. 2005–2009, 2008.
93. J. Hu, X. Ruan, and Y.P. Chen, Thermal Conductivity and Thermal Rectification in Graphene Nanoribbons: a Molecular Dynamics Study, *Nano Letters*, Vol. 9, No. 7, pp. 2730–2735, 2009.
94. Y. Xu, X. Chen, B.-L. Gu, and W. Duan, Intrinsic Anisotropy of Thermal Conductance in Graphene Nanoribbons, *Applied Physics Letters*, Vol. 95, No. 23, p. 233116, 2009.
95. Z. Wei, Y. Chen, and C. Dames, Wave Packet Simulations of Phonon Boundary Scattering at Graphene Edges, *Journal of Applied Physics*, Vol. 112, No. 2, pp. 024328–024328, 2012.
96. S. Chen, Q. Wu, C. Mishra, J. Kang, H. Zhang, K. Cho, W. Cai, A.A. Balandin, and R.S. Ruoff, Thermal Conductivity of Isotopically Modified Graphene, *Nature Materials*, Vol. 11, No. 3, pp. 203–207, 2012.
97. J. Hu, S. Schiffli, A. Vallabhaneni, X. Ruan, and Y.P. Chen, Tuning the Thermal Conductivity of Graphene Nanoribbons by Edge Passivation and Isotope Engineering: A Molecular Dynamics Study, *Applied Physics Letters*, Vol. 97, No. 13, p. 133107, 2010.
98. Z.G. Fthenakis, and D. Tománek, Computational Study of the Thermal Conductivity in Defective Carbon Nanostructures, *Physical Review B*, Vol. 86, No. 12, p. 125418, 2012.
99. D. Dragoman, and M. Dragoman, Giant Thermoelectric Effect in Graphene, *Applied Physics Letters*, Vol. 91, No. 20, p. 203116, 2007.
100. H. Sevinçli, C. Sevik, T. Çağin, and G. Cuniberti, A Bottom-Up Route to Enhance Thermoelectric Figures of Merit in Graphene Nanoribbons, *Scientific reports*, Vol. 3, p. 1228, 2013.
101. G. Stoltz, N. Mingo, and F. Mauri, Reducing the Thermal Conductivity of Carbon Nanotubes below the Random Isotope Limit, *Physical Review B*, Vol. 80, p. 113408, 2009.
102. R.S. Prasher, X.J. Hu, Y. Chalopin, N. Mingo, K. Lofgreen, S. Volz, F. Cleri, and P. Keblinski, Turning Carbon Nanotubes from Exceptional Heat Conductors into Insulators, *Physical Review Letters*, Vol. 102, p. 105901, 2009.
103. H. Zhang, G. Lee, A.F. Fonseca, T.L. Borders, and K. Cho, Isotope Effect on the Thermal Conductivity of Graphene, *Journal of Nanomaterials*, Vol. 2010, p. 537657, 2010.
104. X. Li, J. Chen, C. Yu, and G. Zhang, Comparison of Isotope Effects on Thermal Conductivity of Graphene Nanoribbons and Carbon Nanotubes, *Applied Physics Letters*, Vol. 103, No. 1, p. 013111, 2013.
105. J.-W. Jiang, J. Lan, J.-S. Wang, and B. Li, Isotopic Effects on the Thermal Conductivity of Graphene Nanoribbons: Localization Mechanism, *Journal of Applied Physics*, Vol. 107, No. 5, p. 054314, 2010.
106. A.Y. Serov, Z.-Y. Ong, and E. Pop, Effect of Grain Boundaries on Thermal Transport in Graphene, *Applied Physics Letters*, Vol. 102, No. 3, p. 033104, 2013.
107. A. Cao, and J. Qu, Kapitza Conductance of Symmetric Tilt Grain Boundaries in Graphene. *Journal of Applied Physics*, Vol. 111, No. 5, p. 053529, 2012.

108. A. Bagri, S.-P. Kim, R.S. Ruoff, and V.B. Shenoy, Thermal Transport across Twin Grain Boundaries in Polycrystalline Graphene from Nonequilibrium Molecular Dynamics Simulations, *Nano Letters*, Vol. 11, No. 9, pp. 3917–3921, 2011.
109. Z.-Y. Ong, E. Pop, B. Qiu, and X. Ruan, A Flexural Resonance Mechanism in Graphene-SiO_2 Interfacial Thermal Transport, unpublished.
110. B. Persson, and H. Ueba, Heat Transfer between Graphene and Amorphous SiO_2, *Journal of Physics: Condensed Matter*, Vol. 22, No. 46, p. 462201, 2010.
111. A.K. Vallabhaneni, B. Qiu, J. Hu, Y.P. Chen, A.K. Roy, and X. Ruan, Interfacial Thermal Conductance Limit and Thermal Rectification across Vertical Carbon Nanotube/Graphene Nanoribbon–Silicon Interfaces, *Journal of Applied Physics*, Vol. 113, No. 6, pp. 064311–064311, 2013.
112. P.A. Khomyakov, G. Giovannetti, P.C. Rusu, G. Brocks, J. van den Brink, and P.J. Kelly, First-Principles Study of the Interaction and Charge Transfer between Graphene and Metals, *Physical Review B*, Vol. 79, p. 195425, 2009.
113. R. Mao, B.D. Kong, C. Gong, S. Xu, T. Jayasekera, K. Cho, and K.W. Kim, First-Principles Calculation of Thermal Transport in Metal/Graphene Systems. *Physical Review B*, Vol. 87, p. 165410, 2013.
114. B.A. Cola, J. Xu, C. Cheng, X. Xu, T.S. Fisher, and H. Hu, Photoacoustic Characterization of Carbon Nanotube Array Thermal Interfaces, *Journal of Applied Physics*, Vol. 101, No. 5, p. 054313, 2007.
115. M.A. Panzer, H.M. Duong, J. Okawa, J. Shiomi, B.L. Wardle, S. Maruyama, and K.E. Goodson, Temperature-Dependent Phonon Conduction and Nanotube Engagement in Metalized Single Wall Carbon Nanotube Films, *Nano Letters*, Vol. 10, No. 7, pp. 2395–2400, 2010.
116. D. Wang, M.T. Carlson, and H.H. Richardson, Absorption Cross Section and Interfacial Thermal Conductance from an Individual Optically Excited Single-Walled Carbon Nanotube, *ACS Nano*, Vol. 5, No. 9, pp. 7391–7396, 2011.
117. S. Shin, and M. Kaviany, Interflake Thermal Conductance of Edge-Passivated Graphene, *Physical Review B*, Vol. 84, p. 235433, 2011.
118. L. Hu, T. Desai, and P. Keblinski, Thermal Transport in Graphene-Based Nanocomposite, *Journal of Applied Physics*, Vol. 110, No. 3, p. 033517, 2011.
119. V. Varshney, S.S. Patnaik, A.K. Roy, G. Froudakis, and B.L. Farmer, Modeling of Thermal Transport in Pillared-Graphene Architectures, *ACS Nano*, Vol. 4, No. 2, pp. 1153–1161, 2010.
120. J. Lee, V. Varshney, J.S. Brown, A.K. Roy, and B.L. Farmer, Single Mode Phonon Scattering at Carbon Nanotube-Graphene Junction in Pillared Graphene Structure, *Applied Physics Letters*, Vol. 100, No. 18, p. 183111, 2012.
121. A. Majumdar, and P. Reddy, Role of Electron–Phonon Coupling in Thermal Conductance of Metal–Nonmetal Interfaces, *Applied Physics Letters*, Vol. 84, No. 23, pp. 4768–4770, 2004.
122. Y. Wang, X. Ruan, and A.K. Roy, Two-Temperature Nonequilibrium Molecular Dynamics Simulation of Thermal Transport across Metal-Nonmetal Interfaces, *Physical Review B*, Vol. 85, p. 205311, 2012.
123. X. Li, B.D. Kong, J.M. Zavada, and K.W. Kim, Strong Substrate Effects of Joule Heating in Graphene Electronics, *Applied Physics Letters*, Vol. 99, No. 23, p. 233114, 2011.
124. J. Hu, Y. Wang, A. Vallabhaneni, X. Ruan, and Y.P. Chen, Nonlinear Thermal Transport and Negative Differential Thermal Conductance in Graphene Nanoribbons, *Applied Physics Letters*, Vol. 99, No. 11, p. 113101, 2011.
125. B. Li, L. Wang, and G. Casati, Thermal Diode: Rectification of Heat Flux, *Physical Review Letters*, Vol. 93, p. 184301, 2004.
126. Y. Wang, A. Vallabhaneni, J. Hu, B. Qiu, Y.P. Chen, and X. Ruan, Phonon Lateral Confinement Enables Thermal Rectification in Asymmetric Single-Material Nanostructures, *Nano Letters*, Vol. 14, No. 2, pp. 592–596.
127. C. Starr, The Copper Oxide Rectifier, *Physics*, Vol. 7, No. 1, pp. 15–19, 1936.

128. M. Alaghemandi, F. Leroy, E. Algaer, M.C. Böhm, and F. Müller-Plathe, Thermal Rectification in Mass-Graded Nanotubes: a Model Approach in the Framework of Reverse Non-Equilibrium Molecular Dynamics Simulations, *Nanotechnology*, Vol. 21, No. 7, p. 075704, 2010.
129. N. Yang, G. Zhang, and B. Li, Thermal Rectification in Asymmetric Graphene Ribbons, *Applied Physics Letters*, Vol. 95, No. 3, pp. 033107–033107, 2009.
130. G. Wu, and B. Li, Thermal Rectifiers from Deformed Carbon Nanohorns, *Journal of Physics: Condensed Matter*, Vol. 20, No. 17, p. 175211, 2008.
131. G. Wu, and B. Li, Thermal Rectification in Carbon Nanotube Intramolecular Junctions: Molecular Dynamics Calculations, *Physical Review B*, Vol. 76, p. 085424, 2007.
132. N. Yang, G. Zhang, and B. Li, Carbon Nanocone: a Promising Thermal Rectifier, *Applied Physics Letters*, Vol. 93, No. 24, pp. 243111–243111, 2008.
133. Y. Wang, S. Chen, and X. Ruan, Tunable Thermal Rectification in Graphene Nanoribbons Through Defect Engineering: A Molecular Dynamics Study, *Applied Physics Letters*, Vol. 100, No. 16, pp. 163101–163101, 2012.
134. Q.-X. Pei, Y.-W. Zhang, Z.-D. Sha, and V.B. Shenoy, Carbon Isotope Doping Induced Interfacial Thermal Resistance and Thermal Rectification in Graphene, *Applied Physics Letters*, Vol. 100, No. 10, pp. 101901–101901, 2012.
135. K. Bui, H. Nguyen, C. Cousin, A. Striolo, and D.V. Papavassiliou, Thermal Behavior of Double-Walled Carbon Nanotubes and Evidence of Thermal Rectification, *The Journal of Physical Chemistry C*, Vol. 116, No. 7, pp. 4449–4454, 2012.
136. K. Gordiz, S. Vaez Allaei, and F. Kowsary, Thermal Rectification in Multi-Walled Carbon Nanotubes: A Molecular Dynamics Study, *Applied Physics Letters*, Vol. 99, No. 25, pp. 251901–251901, 2011.
137. A. Rajabpour, S. Vaez Allaei, and F. Kowsary, Interface Thermal Resistance and Thermal Rectification in Hybrid Graphene-Graphane Nanoribbons: A Nonequilibrium Molecular Dynamics Study, *Applied Physics Letters*, Vol. 99, No. 5, pp. 051917–051917, 2011.
138. K.G.S.H. Gunawardana, K. Mullen, J. Hu, Y.P. Chen, and X. Ruan, Tunable Thermal Transport and Thermal Rectification in Strained Graphene Nanoribbons, *Physical Review B*, Vol. 85, p. 245417, 2012.
139. B.-Q. Ai, W.-R. Zhong, and B. Hu, Dimension Dependence of Negative Differential Thermal Resistance in Graphene Nanoribbons, *The Journal of Physical Chemistry C*, Vol. 116, No. 25, pp. 13810–13815, 2012.
140. The Nobel Prize in Chemistry, Nobel Media AB 2013. Web. 19 Mar 2014, available at http://www.nobelprize.org/nobel_prizes/chemistry/laureates/2013/.
141. T.M. Gibbons, and S.K. Estreicher, Impact of Impurities on the Thermal Conductivity of Semiconductor Nanostructures: First-Principles Theory, *Physical Review Letters*, Vol. 102, p. 255502, 2009.
142. T. Luo, and J.R. Lloyd, Ab Initio Molecular Dynamics Study of Nanoscale Thermal Energy Transport, *Journal of Heat Transfer*, Vol. 130, No. 12, p. 122403, 2008.